Journal of Organometallic Chemistry 693 (2008) 3751–3759

Contents lists available at ScienceDirect

Journal of Organometallic Chemistry

journal homepage: www.elsevier.com/locate/jorganchem

Synthesis, characterisation of two hexa-iron clusters with $\{Fe_2S_2(CO)_x\}$ (x = 5 or 6) fragments and investigation into their inter-conversion

Wei Zhong [a], Giuseppe Zampella [b], Zhimei Li [a], Luca De Gioia [b], Yinqiu Liu [c], Xirui Zeng [c], Qiuyan Luo [c], Xiaoming Liu [a,*]

[a] Department of Chemistry, Institute for Advanced Study, Nanchang University, Nanchang, 330031 Jiangxi, China
[b] Department of Biotechnology and Biosciences, University of Milano-Bicocca, 20126 Milano, Italy
[c] School of Chemistry and Chemical Engineering, Jinggangshan University, Ji'an, 343009 Jiangxi, China

ARTICLE INFO

Article history:
Received 15 August 2008
Received in revised form 6 September 2008
Accepted 9 September 2008
Available online 18 September 2008

Keywords:
Hexa-iron clusters
Iron–sulfur–carbonyl complexes
Reaction mechanism
DFT calculations
[FeFe]-hydrogenase

ABSTRACT

Reaction of a trithiol ligand, 2-(mercaptomethyl)-2-methylpropane-1,3-dithiol (**H_3L**), with tri-iron dodecacarbonyl in toluene produces two hexa-iron clusters (**1** and **2**). The two clusters are characterised crystallographically and spectroscopically. NMR spectroscopy reveals that the cluster **2** exists in two conformations in equilibrium $\mathbf{2}_{anti} \Leftrightarrow \mathbf{2}_{syn}$ and the equilibrium constant K_{eq} = 0.55 under CO atmosphere. In the cluster **2**, the central $\{Fe_2S_2(CO)_6\}$ sub-unit is flanked by two identical $\{Fe_2S_2(CO)_6\}$ satellite sub-units through thiolate linkages whereas one of the thiolate linkages can further form Fe–S bond with the proximal Fe atom in one of the two satellite sub-units to produce the cluster **1** by expelling one CO. This conversion can be entirely reversed by continuously purging CO through the solution of the cluster **1**. As suggested by DFT calculations, the conversion features a key step, the rotation of the $Fe_{prox}(CO)_3$ to expose a vacant site for exogenic ligand binding (the S atom from the central sub-unit in this case) with concomitant switch for one of the three CO ligands in the unit of $Fe_{prox}(CO)_3$ from terminal to bridging orientation. The conversion from the clusters **1**–**2** involving one CO uptake is much faster than its reverse process since the latter is an endergonic process characterised by large reaction barriers, as revealed by the DFT calculations.

1. Introduction

Iron–sulfur clusters are found in many forms of life and play an important role in electron transfer and may have catalytic, structural and sensory roles as well [1]. Unlike the iron–sulfur clusters whose biological relevance has well been known, iron–sulfur–carbonyl organometallic units had not been found to have a biological role to play until the revelations that the active sites of three phylogenically unrelated hydrogenases possess iron-sulfur-carbonyl organometallic moieties [2–4]. These metalloenzymes catalyse reversibly and efficiently proton reduction and hydrogen oxidation reactions. The relevance of hydrogen to future energy alternatives has inspired great research interests into the iron-sulfur-carbonyl chemistry [5–13]. We are particularly interested in modelling the iron centres of the [FeFe]- and [Fe]-hydrogenases in attempt to further understand the catalytic chemistry around the enzymes in recent years and achieve artificial systems which may have similar functionalities to the enzymes [14,15].

Inorganic sulfide and organic thiols are common components used in biology to construct iron–sulfur motifs which mainly involve electron transfer. Reactions of thiols and iron-carbonyl precursors afford a large collection of iron–sulfur–carbonyl complexes, which often possess novel structures and exhibit unusual chemical reactivity [16–19]. Trithiol ligand, 2-(mercaptomethyl)-2-methylpropane-1,3-dithiol, **H_3L**, first described by Bosnich and coworkers [20] is a universal ligand reacting with a variety of transition metals [21–23]. Recently, Pickett and co-workers reported the reaction of this ligand with tri-iron dodecacarbonyl generating a unique cluster $[Fe_4\mathbf{L}_2(CO)_8]$ with a $\{Fe^{I}–Fe^{II}–Fe^{II}–Fe^{I}\}$ core [16,24]. Song and co-workers used the same precursors to perform reactions and isolated two different iron-sulfur-carbonyl clusters [25]. In a course of preparing di-iron carbonyl complexes, we further explored this reaction chemistry of this ligand with $Fe_3(CO)_{12}$. Here, we report the synthesis, characterisation and inter-conversion between the two iron–sulfur–carbonyl clusters, $\{[Fe_2(CO)_5\mathbf{L}][Fe_2(CO)_6][\mathbf{L}Fe_2(CO)_6]\}$, **1** and $\{[Fe_2(CO)_6\mathbf{L}]_2[Fe_2(CO)_6]\}$, **2**, isolated from the same reaction. The inter-conversion reaction between the two clusters was probed by using ^{1}H NMR, infrared and UV–Visible spectroscopic techniques as well as theoretical calculations.

* Corresponding author. Tel./fax: +86 0791 3969254.
E-mail address: xiaoming.liu@ncu.edu.cn (X. Liu).

0022-328X/$ - see front matter © 2008 Elsevier B.V. All rights reserved.
doi:10.1016/j.jorganchem.2008.09.021

2. Result and discussion

2.1. Synthesis

The trithiol ligand, **H_3L**, shows diverse reactivity towards a variety of transition metals including iron [16,20–23,25]. This diversity is further demonstrated in this case. When the ratio of the ligand and the iron-carbonyl precursor is 1:1, the isolatable product is the tetra-iron cluster [16]. Increasing the ratio to 1:1.5 leads to the isolation of two iron-sulfur-carbonyl clusters {[$Fe_2(CO)_5$**L**][$Fe_2(CO)_6$][**L**$Fe_2(CO)_6$]} (**1**) and {[$Fe_2(CO)_6$**L**]$_2$[$Fe_2(CO)_6$] (**2**) in 35% and ~3% yields, respectively. It was proposed that the tetra-iron cluster was formed through oxidative elimination of dihydrogen and loss of CO from [$Fe_2(HSCH_2)CMe(CH_2S)_2(CO)_5$] [16]. The precursor of forming this pentacarbonyl complex is probably a hexacarbonyl intermediate, [$Fe_2(HSCH_2)CMe(CH_2S)_2(CO)_6$], in which unlike the pentacarbonyl complex, the pendant thiol is free for further coordination. When excess tri-iron dodecacarbonyl is present, this hexacarbonyl complex with a free pendant thiol acts possibly as a free thiol and readily reacts with the tri-iron dodecacarbonyl to form a hexacarbonyl complex. In fact, the reaction of this kind is an effective way to synthesise di-iron hexacarbonyl model complexes for the di-iron centre of the H-cluster of the [FeFe]-hydrogenase [9,10,13,26]. In this case, the di-iron core has two satellite di-iron sub-units which come along with the "free" thiol, Scheme 1.

Albeit the cluster **1** is thermodynamically unfavoured compared to the cluster **2**, as indicated by DFT calculations (*vide infra*), it is the predominant product in the reaction. This anomaly is possibly attributed to the harsh reaction temperature and lacking adequate presence of CO. Flash chromatography failed to produce absolutely pure form of the cluster **1** since trace amount of the other cluster was always present due to the equilibrium between the two in solution. Fortunately, analytically pure product could be obtained *via* recrystallisation. The cluster **1** crystallised readily as dark-brown crystal blocks from a solution of acetonitrile under Ar atmosphere. Due to the low yield of the cluster **2** in the reaction, adequate quantity of this cluster for further characterisation was produced by converting the cluster **1** upon purging CO through its solution of dichloromethane. The cluster **2** crystallised as red crystals from the same solvent as used for the cluster **1** under CO atmosphere. These crystals were all suitable for X-ray single crystal diffraction analysis.

The two clusters have seemingly complicated infrared spectra showing multi absorption bands between 1900 and 2100 cm^{-1}. However, close examination reveals that the infrared spectrum of the cluster **2** comprises characteristic spectral features of di-iron hexacarbonyl complexes, for instance, [Fe_2(pdt)$(CO)_6$] (pdt = propanedithiolate), which shows absorption bands at 2074, 2035 and 1994 cm^{-1} [27]. For the infrared spectrum of the cluster **1**, in addition to the characteristic spectral features of the di-iron hexacarbonyl complexes, three absorption bands around 2040, 1980 and 1930 cm^{-1} for di-iron pentacarbonyl complexes are also evident, particularly the much weak band at the lowest frequency which is a distinct feature for di-iron pentacarbonyl complexes [14,28].

2.2. Crystallographic analysis

The crystal structures of the clusters **1** and **2** are shown in the style of capped sticks for clarity reason, Fig. 1. The crystallographic details and selected bonding parameters are tabulated in Tables 1 and 2, respectively. For the cluster **2**, there is a pseudo-C_2 rotating axis which equally divides and is perpendicular to the Fe–Fe bond of the central sub-unit. This axis also goes through a plane which bisects the angle composed by the two equatorial CO and the iron atom in the central sub-unit. The definition pseudo-C_2 axis stems from the observation that the two sub-units are not strictly identical in solid state and differences in some of the bonding parameters

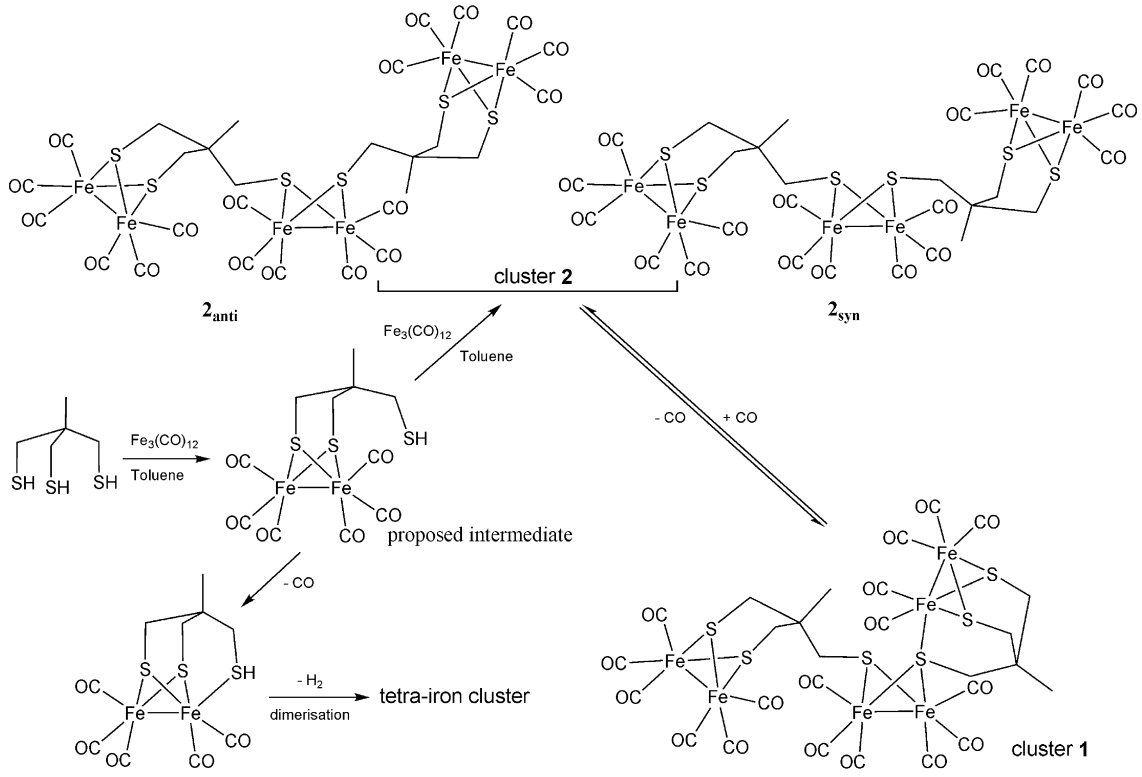

Scheme 1. The syntheses of the two clusters **1** and **2** and the tetra-iron cluster.

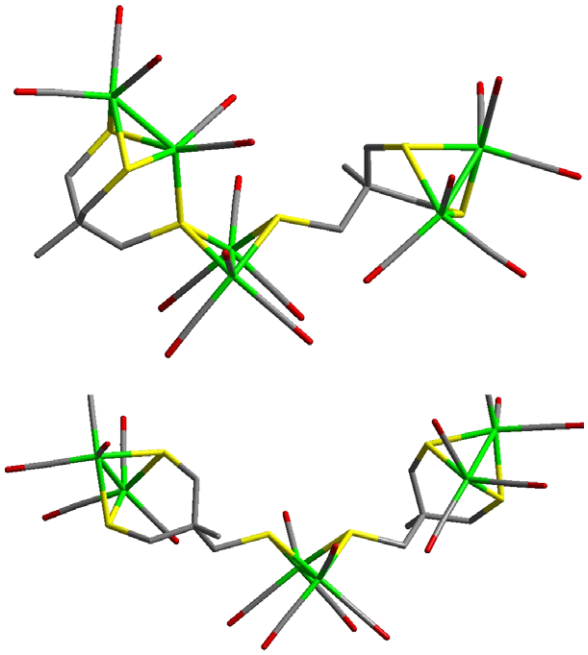

Fig. 1. The structural views of the clusters **1** (top) and **2** (bottom) with colour legend: green = Fe; yellow = S; red = O and grey = C (hydrogen atoms are omitted for clearer view). (For interpretation of the references in colour in this figure legend, the reader is referred to the web version of this article.)

for the two satellite sub-units are beyond crystallographic errors, as shown in Table 2.

The Fe–Fe distances related to the $\{Fe_2S_2(CO)_6\}$ sub-unit in the two clusters are 2.503 ± 0.007 Å, whereas this metal-metal distance in the $\{Fe_2S_2(CO)_5\}$ sub-unit in the cluster **1** is slightly longer (2.520 Å). These values are in good agreement with those found in di-iron hexacarbonyl and pentacarbonyl complexes [14,29,30]. The statistic value for all Fe–S bond lengths in the two clusters is 2.264 Å with a deviation of 0.009 Å and no significant differences are found compared to those for di-iron hexacarbonyl and pentacarbonyl complexes [14,29,30]. Under the constraints from the ligand frames, the bonding angles ∠S–Fe–S in the two satellite di-iron sub-units are about 85° with a few degrees of deviation, which is approximately 10° larger compared to the bond angles of the central sub-units where no such bonding constraints exist in both clusters. These values are again generally in accordance with corresponding values for the di-iron hexacarbonyl and pentacarbonyl complexes [14,29,30].

Notably, the chemical integration of three sub-units of $\{Fe_2S_2\}$ does show some impacts on their overall structures. In the cluster **1**, the two Fe–S bonds of the central sub-unit $\{Fe_2S_2(CO)_6\}$ next to the $\{Fe_2S_2(CO)_5\}$ sub-unit are 0.01 Å shorter than the other two Fe–S bonds. This bond shortening is probably caused by the coordination of the S atom to form the $\{Fe_2S_2(CO)_5\}$ sub-unit. Due to steric repulsions, the bond angles ∠C–Fe–Fe composed by the apical CO ligand and the Fe–Fe bonds fall into two distinct categories, (149.5 ± 1.8)° for the distal $Fe_{dist}(CO)_3$ units in the two satellite di-iron sub-units with less steric repulsion and (159.2 ± 1.7)° for the proximal $Fe_{prox}(CO)_3$ units with stronger repulsion from the surrounding chemical moieties in both clusters. For the central sub-units in these two clusters, these bond angles fall also in the latter category due to bulkiness of its two satellite sub-units.

2.3. The conformations of the two clusters in solution

The chemical shifts of the proton NMR in di-iron carbonyl complexes derived from the ligand **H_3L** and its derivative show great sensitivity towards subtle variations in coordinations as well as conformations [16,25,28,31]. Among the signals, the chemical shift for the methyl group is particularly a useful handle in probing the

Table 1
Crystallographic details for the clusters **1** and **2**

	$C_{27}H_{18}Fe_6O_{17}S_6$, cluster **1**	$C_{28}H_{18}Fe_6O_{18}S_6$, cluster **2**
Formula weight	1141.94	1169.95
Temperature (K)	293(2)	293(2)
Wavelength (Å)	0.71073	0.71073
Crystal system	Monoclinic	Triclinic
Space group	*P*21/*n*	$P\bar{1}$
Unit cell dimensions		
a (Å)	9.1276(11)	9.1876(13)
b (Å)	30.299(4)	15.137(2)
c (Å)	14.5989(17)	17.432(3)
α (°)	90	99.842(2)
β (°)	94.240(2)	0.327(2)
γ (°)	90	95.487(2)
Volume (Å^3)	4026.4(9)	2377.1(6)
Z	4	2
D_{calc} (Mg/m^3)	1.884	1.635
Absorption coefficient (mm^{-1})	2.484	2.108
F(000)	2272	1164
Crystal size (mm)	0.38 × 0.15 × 0.11	0.40 × 0.15 × 0.12
θ Range for data collection (°)	1.94–25.50	1.96–25.50
Limiting indices	$-10 \leqslant h \leqslant 10$, $-36 \leqslant k \leqslant 36$, $-17 \leqslant l \leqslant 17$	$-11 \leqslant h \leqslant 9$, $-18 \leqslant k \leqslant 18$, $-21 \leqslant l \leqslant 21$
Reflections collected/unique, R_{int}	25 102/7436	14854/8110
	0.0706	0.0248
Completeness (%) to θ = 25.50	99.2	91.6
Absorption correction	None	None
Maximum and minimum transmission	0.7465 and 0.4218	0.776 and 0.691
Refinement method	Full-matrix least-squares on F^2	Full-matrix least-squares on F^2
Goodness-of-fit on F^2	0.813	0.996
Final *R* indices [$I > 2\sigma(I)$]	R_1 = 0.0329, wR_2 = 0.0543	R_1 = 0.0729, wR_2 = 0.2357
R indices (all data)	R_1 = 0.0682, wR_2 = 0.0565	R_1 = 0.1027, wR_2 = 0.2754
Largest difference in peak and hole (e Å^{-3})	0.405 and −0.406	1.853 and −0.521

Table 2
Selected bond lengths (Å) and angles (°)[a]

Cluster **1**		Cluster **2**	
Fe(1)–Fe(2)	2.4979(9)	Fe(1)–Fe(2)	2.5041(17)
Fe(3)–Fe(4)	2.5125(8)	Fe(3)–Fe(4)	2.5061(15)
Fe(5)–Fe(6)	2.5196(9)	Fe(5)–Fe(6)	2.4972(17)
Fe(1)–S(1)	2.2655(12)	Fe(1)–S(1)	2.261(2)
Fe(1)–S(2)	2.2579(12)	Fe(1)–S(2)	2.260(2)
Fe(2)–S(1)	2.2617(13)	Fe(2)–S(1)	2.253(2)
Fe(2)–S(2)	2.2597(12)	Fe(2)–S(2)	2.255(3)
Fe(3)–S(3)	2.2746(12)	Fe(3)–S(3)	2.282(2)
Fe(3)–S(4)	2.2666(12)	Fe(3)–S(4)	2.267(2)
Fe(4)–S(3)	2.2746(12)	Fe(4)–S(3)	2.273(2)
Fe(4)–S(4)	2.2645(12)	Fe(4)–S(4)	2.276(2)
Fe(5)–S(5)	2.2491(12)	Fe(5)–S(5)	2.279(2)
Fe(5)–S(6)	2.2474(12)	Fe(5)–S(6)	2.267(2)
Fe(6)–S(5)	2.2661(13)	Fe(6)–S(5)	2.256(2)
Fe(6)–S(6)	2.2565(14)	Fe(6)–S(6)	2.268(2)
Fe(5)–S(4)	2.2578(12)		
S(1)–Fe(1)–S(2)	83.80(4)	S(1)–Fe(1)–S(2)	83.70(8)
S(1)–Fe(2)–S(2)	83.85(4)	S(1)–Fe(2)–S(2)	83.98(9)
S(3)–Fe(3)–S(4)	75.96(4)	S(3)–Fe(3)–S(4)	74.50(8)
S(3)–Fe(4)–S(4)	76.00(4)	S(3)–Fe(4)–S(4)	74.50(7)
S(5)–Fe(5)–S(6)	86.73(4)	S(5)–Fe(5)–S(6)	82.91(8)
		S(5)–Fe(6)–S(6)	83.38(8)
S(4)–Fe(5)–S(6)	96.74(5)		
S(4)–Fe(5)–S(5)	94.09(4)		
S(5)–Fe(6)–S(6)	86.11(5)		
C(6)–Fe(2)–Fe(1)	146.49(15)	C(2)–Fe(1)–Fe(2)	147.6(3)
C(22)–Fe(6)–Fe(5)	146.40(18)	C(26)–Fe(6)–Fe(5)	149.8(3)
C(13)–Fe(3)–Fe(4)	151.01(14)	C(13)–Fe(3)–Fe(4)	150.4(3)
C(16)–Fe(4)–Fe(3)	150.64(14)	C(16)–Fe(4)–Fe(3)	150.9(3)
C(2)–Fe(1)–Fe(2)	158.15(14)	C(6)–Fe(2)–Fe(1)	158.3(3)
		C(23)–Fe(5)–Fe(6)	161.2(3)

[a] In both clusters, Fe(3) and Fe(4) are from the central sub-unit and in the cluster **2**, Fe(2) and Fe(5) are proximal to S(3) and S(4) atoms of the central sub-unit respectively. But in the cluster **1**, Fe(5) is bound to S(4) and Fe(1) is proximal to S(3).

orientation of the two di-iron sub-units around the central one. These signals show doublet-doublet signal pattern for each CH_2 group due to cyclic effect and singlet for the methyl group. The NMR spectra of the two clusters are shown in Fig. 2. As shown in Fig. 2 (top), the cluster **1** shows two singlet peaks at 0.873 and 1.222 ppm, one for the methyl group from the pentacarbonyl (5CO) sub-unit and the other from hexacarbonyl (6CO) sub-unit. By analogy, we assign the peaks at 0.873, 1.745, 2.383 and 2.282 ppm to the 5CO sub-unit and the peaks at 1.222, 2.193, 2.644 and 2.683 ppm to the 6CO sub-unit.

The cluster **2** shows more complicated ^{1}H NMR spectrum compared to that of the cluster **1**, Fig. 2 (bottom). The three well-resolved resonance peaks for methyl group fall into the range defined by the two resonance peaks observed for the cluster **1**. This is clearly shown in aligned and simplified schematic view of the spectral signals of the two clusters, Fig. 3. Furthermore, the intensity of the central peak increases whereas the intensities for the other two decrease with the increase in the concentration of CO in solution. Moreover, for the latter two peaks, they show essentially equal intensities either in high or low CO concentrations, Fig. S1a. This shows that the two signals originate from one species. Finally, the 2:1 ratio of the total signal integration of the methylene groups over that of the methyl groups tells that the organic backbone is intact and no impurities are involved in the solution of the cluster **2** when the NMR measurements were conducted. These observations strongly suggest that in solution, the cluster **2** exists in two conformations which are in equilibrium.

It is well known that complexes of the motif, $\{Fe_2(SR)_2(CO)_6\}$, shows three possible isomers with regard to the orientations of the two S–R bonds, *syn*, *anti* and *syn*′ [32–34]. In this case, the R is the 6CO sub-unit. Thus the cluster **2** could take equatorial–equatorial (*syn* isomer), apical–equatorial (*anti* isomer) and apical–apical conformations (*syn*′ isomer). Due to the bulkiness, the *syn*′ isomer is unlikely to exist. For the *syn* isomer, $\mathbf{2}_{syn}$, more or less like the conformation as revealed in its solid state, the two sub-units are chemically identical in solution. The resonance peak at 1.011 ppm is assigned to this isomer, $\mathbf{2}_{syn}$. The other five related peaks are identified by the correlation between their intensities and the concentration of CO, Fig. 3e. The other form must be the *anti* isomer, $\mathbf{2}_{anti}$ showing two types of signals for both CH_2 and CH_3 groups, Fig. 3c and d. The equilibrium constant for $\mathbf{2}_{anti} \Leftrightarrow \mathbf{2}_{syn}$ is estimated as 0.55 ± 0.01 by using the intensities of the resonance signals of the methyl groups in a solution of deuterated chloroform under CO atmosphere. Thus, the Gibbs free energy for this equilibrium is approximately 1.5 kJ mol^{-1} (298 K) showing the easiness of conversion from one to the other and that $\mathbf{2}_{syn}$ is slightly thermodynamically less favoured compared to the other isomer $\mathbf{2}_{anti}$, which is in agreement with those reported in literature [32].

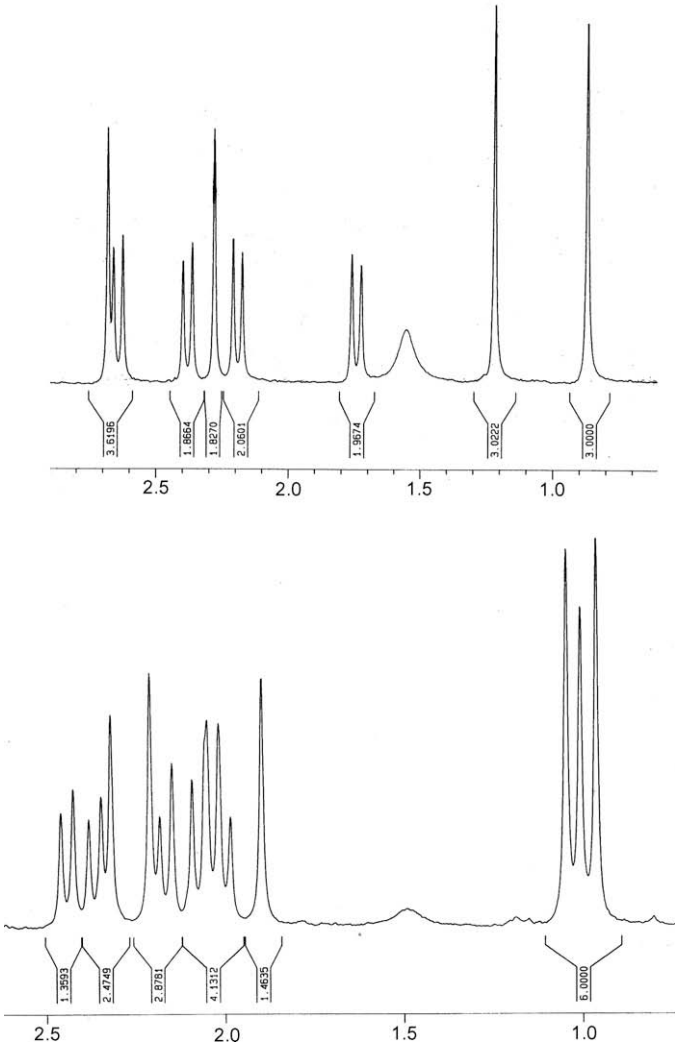

Fig. 2. The ^{1}H NMR spectra of the two clusters, **1** (top) and **2** (bottom).

2.4. Inter-conversion between the clusters *1* and *2*

Purging the solution of the cluster **1** in dichloromethane with CO leads to complete conversion of this cluster to the cluster **2** as evidenced by infrared spectral changes within 2 h, Fig. 4. The conversion accompanies distinct colour change, from dark-brown to bright-red. This colour change is echoed by the changes in their

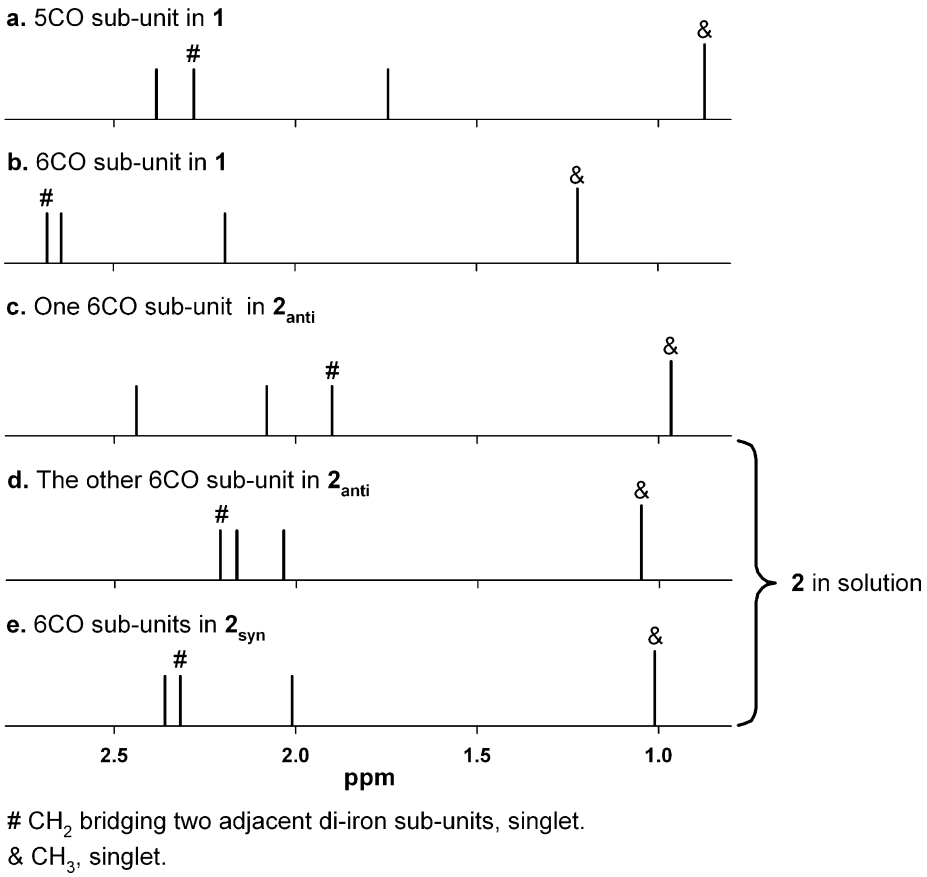

Fig. 3. ^{1}H NMR ($CDCl_3$) chemical shifts distribution of the methyl and methylene groups of the clusters **1** (a and b) and **2** (c–e) (please note that mean values are used for all doublets for clarity. These doublets have average coupling constant of 14 Hz).

UV/Vis spectra during the conversion, Fig. 5. The featured band for di-iron pentacarbonyl complexes near 400 nm [35] decreases while the band at higher frequency gains intensity. The latter spectral absorption band is characteristic feature for di-iron hexacarbonyl complexes [36,37]. Under Ar atmosphere, the opposite process can occur in the solution of the cluster **2**. This reverse process is completed by driving out CO through continuously purging the solution of the cluster **2** with Ar but it is much harder and takes much longer time. This is consistent with the prediction of DFT calculations that the conversion from the cluster **2** to the cluster **1** is a thermodynamically uphill process (*vide infra*). Since the cluster **2** in

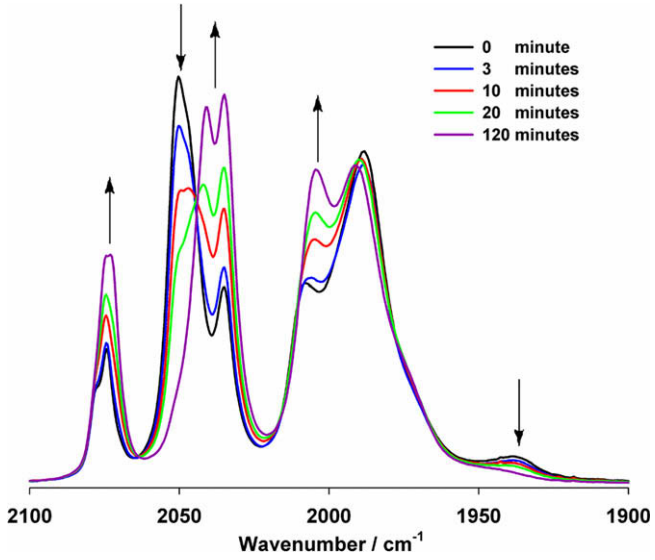

Fig. 4. IR spectral changes with the time of purging CO through the solution during the conversion from the cluster **1** to the cluster **2** in dichloromethane at room temperature.

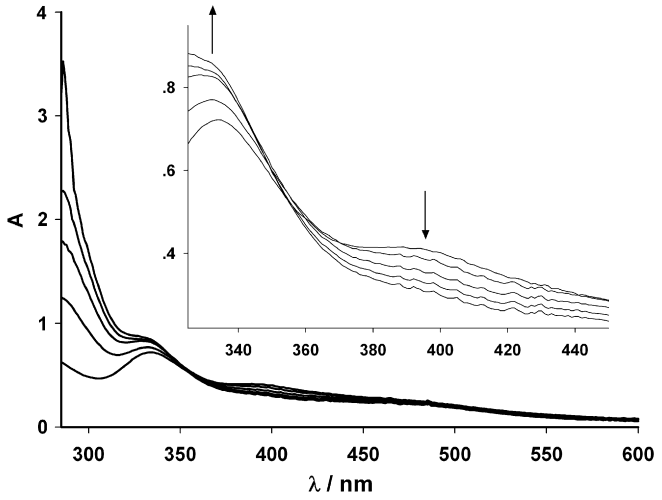

Fig. 5. UV/Vis spectral changes with the time of purging CO through the solution during the conversion from the cluster **1** to the cluster **2** in acetonitrile at room temperature.

solution shows two conformations, three species detectable by NMR are involved in the inter-conversion. Indeed, a solution of the cluster **2** in deuterated chloroform under Ar atmosphere shows significant presence of the cluster **1** *(Fig.* S1b) after being stored overnight at room temperature. Under CO atmosphere, the content of the cluster **1** may be under the detection limit by NMR spectroscopy, normally millimolar.

It has been reported that substitution reactions involving $Fe(CO)_3$ moiety follows the pathway: rotation of the moiety to expose a vacant site, concomitant CO-binding mode switching and substrate binding to the exposed vacant site [38,39]. The conversion from the clusters **2** to **1** proceeds probably in a similar manner.

2.5. DFT calculations

To further elucidate the inter-conversion between the two clusters, DFT calculations have been carried out. To simplify the calculations, a simpler model of the original system has been employed, assuming that the reaction from the clusters **1**–**2** occurs mainly through the central 6CO sub-unit and one of its satellite sub-units, while the other one acts roughly as a "spectator". A visual inspection of the X-ray crystal structure of the clusters **1** and **2** (Fig. 1) justifies such an assumption. Thus, one of the satellite sub-units was substituted with a capping CH_3 group throughout the calculations. In the discussion of DFT data related to the inter-conversion mechanism, the satellite di-iron sub-unit is designated as **A** and the central sub-unit as **B**.

DFT calculations allowed to identify two almost isoenergetic structures for the cluster **2**, one of them is pictured in Fig. 6a, designated as $\mathbf{2_{DFT}}$ to differentiate it from the cluster **2**, whereas the other is shown in *Fig.* S2. These two isomers originate from free rotation around the bond, (**B**) SH_2C–C (tertiary C of **A**), designated as C_B–C_A bond hereafter. As anticipated before, one of the conformations identified by DFT closely corresponds to the solid state structure of the cluster **2**, Fig. 1 (bottom) and Fig. 6a. Starting from this conformation, a two-steps reaction pathway passing through a high energy intermediate species **[2–1]** has been found. Fig. 7 shows the free energy profile for the reaction coordinate, while DFT structures of reactants, intermediate species and transition states are shown in Fig. 6.

As shown in Fig. 6, it turns out that the rotation around the C_B–C_A bond is crucial for the reaction. In fact, rotation around this bond brings the proximal Fe (Fe_{prox}) into a suitable position to interact with the S atom (S_B) which bridges the sub-units **A** and **B**. As observed in **TS1**, the rotation of the $Fe_{prox}(CO)_3$ unit exposes a vacant site to host the incoming S_B atom and concomitantly brings one of the equatorial CO ligands of the $Fe_{prox}(CO)_3$ group into a position suited to interact with the distal Fe atom (Fe_{dist}) of the sub-unit **A** (Fig. 6b). The high energy intermediate species **[2–1]**, Fig. 6c, features an asymmetric μ-CO bridge between the two Fe atoms of the **A** subunit (Fe_{prox}–CO: 1.872 Å; Fe_{dist}–CO: 2.093 Å). In **[2–1]**, the S_B–Fe_{prox} bond is as long as 2.752 Å, probably due to the unusual tri-coordination of the S atom, which links the sub-units **A** and **B**.

Subsequently, the intermediate **[2–1]** evolves to the product $\mathbf{1_{DFT}}$ *via* another transition state, **TS2**, Fig. 7 and Fig. 6d. Unlike **TS1**, the components of the transition eigenvector do not correspond to rotation of the $Fe_{prox}(CO)_3$ moiety, but are mainly composed by the stretching of the breaking bond, *i.e.*, OC_{axial}–Fe_{dist}.

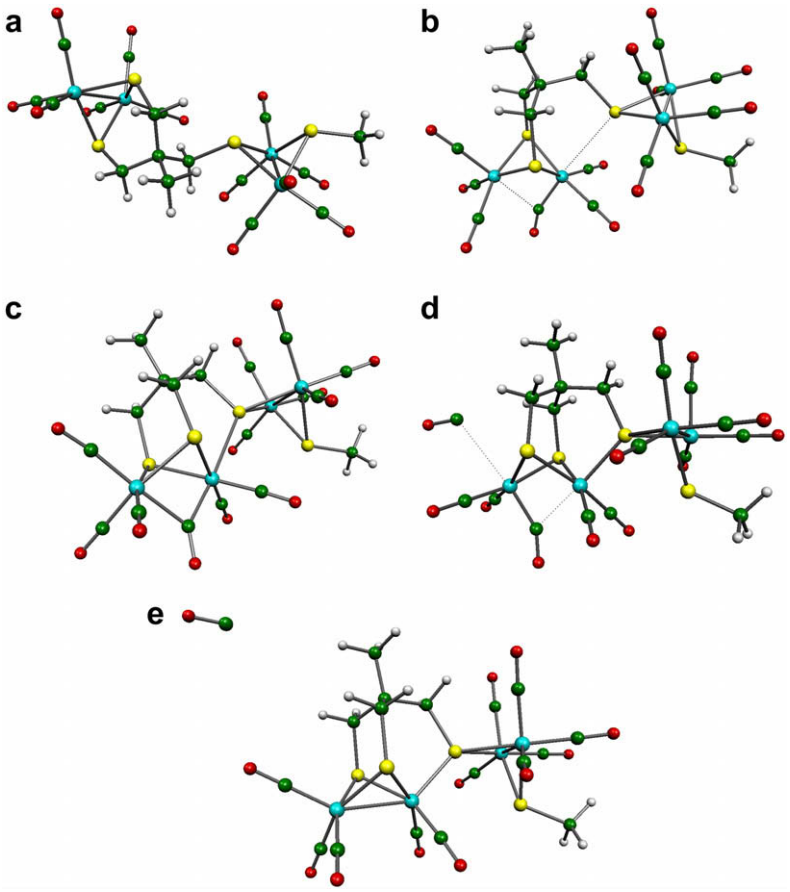

Fig. 6. DFT optimised conformations of (a) $\mathbf{2_{DFT}}$ which closely resembles the solid state structure of the cluster **2**, (b) the first transition state, **TS1**, (c) the high energy intermediate, **[2–1]**, (d) the second transition state, **TS2** and (e) $\mathbf{1_{DFT}}$ which is structurally related to the cluster **1** (colour legend: red = O; green = C; yellow = sulphur; white = H; cyan = Fe). (For interpretation of the references in colour in this figure legend, the reader is referred to the web version of this article.)

This is reminiscent of the transition state structure for CO loss, as identified by DFT calculations in a previous investigation on the CO substitution mechanism of a {2Fe3S} complex related to the [FeFe]-hydrogenase cofactor [40].

Moreover, it must be pointed out that the distance between Fe_{prox} and the tri-coordinated S_B atom shortens to 2.339 Å, compared to the distance between the same atoms observed in **[2–1]** (2.752 Å). This behaviour may stem from the preference of Fe(I) for penta-coordination geometry with respect to the hexa-coordination observed in the **[2–1]**.

The structure of the final 5CO species $\mathbf{1_{DFT}}$, Fig. 6e, has been energy-optimized as a van der Waals complex with CO, in order to avoid energy overestimation coming out from summation at infinite distance of the two molecule energy values. The computed structure $\mathbf{1_{DFT}}$ well reproduces the structural features as observed in the solid state of the cluster **1**. The structural similarities are also reflected by the close correspondence between calculated and experimental IR absorption bands, Table 3. In $\mathbf{1_{DFT}}$, the bond between the tri-coordinated bridging S_B atom and Fe_{prox} atom of **A** sub-unit comes to a more standard value of 2.253 Å. Thermodynamic data indicate that $\mathbf{1_{DFT}}$ is 11.7 kJ mol^{-1} higher in energy than **[2–1]**, Fig. 7.

During the conversion from $\mathbf{2_{DFT}}$ to $\mathbf{1_{DFT}}$ the Gibbs free energy increases by 62.7 kJ mol^{-1} and the largest contribution comes from the step from $\mathbf{2_{DFT}}$ to **[2–1]** (51 kJ mol^{-1}). Thus, the entire conversion from $\mathbf{2_{DFT}}$ to $\mathbf{1_{DFT}}$ is thermodynamically uphill and the rate-limiting step is from $\mathbf{2_{DFT}}$ to **[2–1]**. This result is consistent with the experimentally observed slowness for this converting process.

In summary, two hexa-iron clusters **1** and **2** were synthesised from the reaction of the tripodal ligand (**H_3L**) with $Fe_3(CO)_{12}$. The cluster **2** exists in two isomers, $\mathbf{2}_{syn}$ and $\mathbf{2}_{anti}$, as revealed by NMR spectroscopy. These two clusters undergo reversible inter-conversion through concomitant Fe–S formation and CO cleavage. The conversion from the cluster **1** to the cluster **2** involving one CO uptake is much faster than its reverse process since the latter is an endergonic process characterised by large reaction barriers, as revealed by the DFT calculations. The converting process from the clusters **2** to **1** features the rotation of proximal $Fe_{prox}(CO)_3$ unit which exposes a vacant site for substrate binding (in this case, the incoming S_B atom from the central di-iron sub-unit) with concomitant switch from terminal CO to bridging CO. The DFT calculations suggest a two-step reaction mechanism for the inter-conversion involving two transition states (**TS1** and **TS2**) and one intermediate species, **[2–1]**.

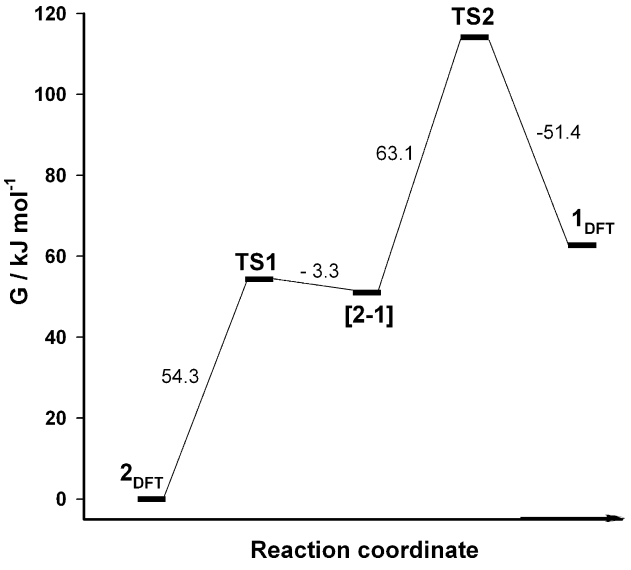

Fig. 7. Energy (G) profile for the proposed reaction pathway of the conversion from $\mathbf{2_{DFT}}$ to $\mathbf{1_{DFT}}$.

Table 3
The computed and experimental IR absorption bands for the clusters **1** and **2**

Cluster **1**		Cluster **2**	
Computed	Experimental	Computed	Experimental
2133.7			2078.1
			2074.2
			2071.7
	2077.4	2057.5	
	2073.4		
2059.5	2048. 7	2031.7	2040.1
2042.4	2043. 0	2025.7	2034.2
2032.5	2034.5	2007.6	2003.6
2003.5	2007.8	1995.2	
1993.9		1990.8	1990.2
		1988.2	
		1982.7	
1989.2	1987.4	1978.8	
1985.5		1974.9	1972.8
1983. 0		1969.1	
1975.4			
1967.9	1966.6		
1958.1			
	1935.2		

3. Experimental

All reactions were carried out under an argon atmosphere using standard Schlenk techniques. Solvents for reactions and electrochemistry were freshly distilled by using appropriate drying agents prior to use. Infrared data were collected on Scimitar 2000 (Varian). ^{1}H NMR spectra were recorded on AVANCE DRX 400 (Bruker). Agilent 8453 was used for UV/Vis spectra collection. Micro-analysis service was provided by Nanjing University (Heraeus CHN-O-Rapid).

Trithiol ligand, 2-(mercaptomethyl)-2-methylpropane-1,3-dithiol (**H_3L**), was prepared by following literature procedures [28].

3.1. Synthesis of the clusters *1* and *2*

$Fe_3(CO)_{12}$ (952 mg, 1.89 mmol) and the ligand **H_3L** (212 mg, 1.26 mmol) were dissolved in freshly distilled toluene (32 ml) and then heated at 85 °C for 120 min. The dark-green mixture turned to red–brown. The toluene was removed and the crude product was purified by flash chromatography using gradient eluents (first hexane and then petroleum ether:ethyl acetate = 20:1, 15:1 and 12:1) to give an orange solid (**2**) (45 mg, 3%) and a red–brown solid (**1**) (501 mg, 35%). A solution of the cluster **2** in acetonitrile at −24 °C produced red single crystals suitable for X-ray single crystal diffraction analysis. Micro-analysis for $C_{28}H_{18}Fe_6O_{18}S_6$ (MW = 1169.89), Calc. C, 28.75; H, 1.55. Found: C, 28.70; H, 1.60%. ^{1}H NMR ($CDCl_3$): 0.966 (3H, s, –C*H*$_3$, 6CO′*), 1.011 (3H, s, –C*H*$_3$, 6CO′), 1.050 (3H, s, –C*H*$_3$, 6CO″), 1.900 (2H, s, –C*H*$_2$SFe, 6CO″*), 2.010 (2H, d, J = 13.8 Hz, 2 × C*H*SFe, 6CO′), 2.035 (2H, d, J = 13.6 Hz, 2 × C*H*SFe, 6CO″), 2.080 (2H, d, J = 13.8 Hz, 2 × C*H*SFe, 6CO″*), 2.164 (2H, d, J = 13.7 Hz, 2 × C*H*SFe, 6CO″), 2.210 (2H, s, –C*H*$_2$SFe, 6CO″), 2.318 (2H, s, –C*H*$_2$SFe, 6CO′), 2.360(2H, d, J = 13.8 Hz, 2 × C*H*SFe, 6CO′), 2.439 (2H, d, J = 13.7 Hz, 2 × C*H*SFe, 6CO″*). Here, the designations, 6CO″* and 6CO″ refer to the 6CO sub-unit which has close contact with the central di-iron sub-unit and the other 6CO sub-unit in the species $\mathbf{2}_{anti}$, respectively, and 6CO′ to the two 6CO sub-units in the species $\mathbf{2}_{syn}$. IR (dichloromethane) ν_{max}/cm^{-1} (CO): 2074.2, 2071.8, 2040.1, 2034.3, 2003.6 and 1990.2.

The cluster **1** was dissolved in acetonitrile and storing the solution in a fridge led to the formation of dark-red single crystals. These crystals were suitable for X-ray single crystal diffraction determination. Micro-analysis for $C_{27}H_{18}Fe_6O_{17}S_6$ (MW = 1141.88), Calc. C, 28.40; H, 1.59. Found: C, 28.30; H, 1.45%. ^{1}H NMR ($CDCl_3$): 0.873 (3H, s, –C*H*$_3$, 5CO), 1.222 (3H, s, –C*H*$_3$, 6CO), 1.745 (2H, d, *J = 14.0* Hz, 2 × C*H*SFe, 5CO), 2.193 (2H, d, *J* = 13.9 Hz, 2 × C*H*SFe, 6CO), 2.282 (2H, s, –C*H*$_2$SFe, 5CO), 2.383 (2H, d, *J* = 14.0 Hz, 2 × C*H*SFe, 5CO), 2.644 (2H, d, *J = 14.0* Hz, 2 × C*H*SFe, 6CO), 2.683 (2H, s, −C*H*$_2$SFe, 6CO). Please note that 5CO and 6CO refer to the 5CO and 6CO sub-units in the cluster **1**, respectively. IR (dichloromethane), ν_{max}/cm^{-1} (CO): 2077.4, 2073.4, 2048.4, 2034.5, 2007.3, 1987.6 and 1935.7.

3.2. X-ray structure determinations

Standard procedures were used for mounting the crystals on a Bruker Apex-II area-detector diffractometer at 293 K. The crystals were routinely wrapped with paraffin oil before being mounted. Intensity data were collected using Mo Kα radiation (λ = 0.71073Å) under 293 K using a phi- and omega- scans mode. The SAINT and SADABS programs in the APPEX(II) software package were used for integration and absorption correction [41]. The structure were solved by direct method using SHELXS-97 program [42] and refined on F^2 with XSHELL6.3.1, all non-hydrogen atoms being modeled anisotropically. All hydrogen atoms were positioned geometrically and treaded as riding on their parent atoms with C–H distances of 0.97 Å (ethyl) and 0.96 Å (methyl), and with U_{iso}(H) = 1.2U_{eq}(C) (ethyl) but U_{iso}(H) = 1.5U_{eq}(C) (methyl).

3.3. Inter-conversion between the clusters *1* and *2*

A solution of **1** (20 mg, 0.018 mmol) in dry dichloromethane (5 ml) was purged continuously with CO for 2 h and the conversion from the clusters **1** to **2** was quantitatively completed. A large scale of the cluster **2** was prepared in this manner since the yield for this cluster is low from the direct synthesis. The reverse process was achieved by continuously purging the solution with Ar for 2 days. For both processes, solvent is added when needed to compensate the solvent loss during the purging due to solvent evaporation.

3.4. DFT calculations

Theoretical calculations were performed by using DFT/B-P86 [43,44] along with a high quality basis set, which includes a triple set of basis function for the valence shell plus a polarization function for each atom (TZVP, according to the nomenclature used by TURBOMOLE package) [45,46]. All stationary points on the DFT energy hypersurface (PES) have been characterised by means of analytical Hessian matrix calculations, which has allowed us to identify such points as either reactants, products or intermediates (no negative eigenvalue of the Hessian matrix, *i.e.* the PES curvature is positive in all directions), or, alternatively, as transition state structures, whenever a first-order saddle point has been identified (*i.e.* only a single eigenvector – the transition vector- is associated to an imaginary vibration frequency, namely to a negative eigenvalue). Transition state structures have been located by means of a quasi-Newton–Raphson method [47], basically consisting in:

(1) Guessing those modes forming the reaction coordinate and keeping them frozen during the energy minimization of all the other structural degrees of freedom.
(2) Calculating the Hessian matrix of such point and determining if the curvature there shows only a single direction (mode) with negative eigenvalue (imaginary frequency).
(3) If requirement in (2) is fulfilled, then one has to "follow" the transition eigenvector, which implies maximizing the energy with respect to the direction indicated by the transition vector, and simultaneously minimizing the energy itself in all other directions.

No implicit solvent model has been considered. Approximated thermodynamic corrections have been added to the DFT electronic energy in order to estimate the Gibbs free energy. To this aim, the partition function of the system (*Q*) associated with nuclear vibrations, rotations and translations has been evaluated for each species on the reaction coordinate, under the ideal gas assumption and under the approximation which treats the total *Q* simply as the product of the single component terms ($q_{vibrational}$, $q_{rotational}$ and $q_{translational}$).

Acknowledgements

We thank the Natural Science Foundation of China (Grant No. 20571038) and the State Key Laboratory of Coordination Chemistry at Nanjing University (China) for supporting this work.

Appendix A. Supplementary data

CCDC 698177 and 698178 contain the supplementary crystallographic data for the clusters **1** and **2,** respectively. These data can be obtained free of charge from The Cambridge Crystallographic Data Centre via www.ccdc.cam.ac.uk/data_request/cif.

Supplementary data associated with this article can be found, in the online version, at doi:10.1016/j.jorganchem.2008.09.021.

References

[1] R.H. Holm, P. Kennepohl, E.I. Solomon, Chem. Rev. 96 (1996) 2239.
[2] R.P. Happe, W. Roseboom, A.J. Pierik, S.P.J. Albracht, K.A. Bagley, Nature 385 (1997) 126.
[3] J.W. Peters, W.N. Lanzilotta, B.J. Lemon, L.C. Seefeldt, Science 282 (1998) 1853.
[4] S. Shima, R.K. Thauer, Chem. Rec. 7 (2007) 37.
[5] M.Y. Darensbourg, E.J. Lyon, J.J. Smee, Coord. Chem. Rev. 206 (2000) 533.
[6] R.B. King, T.E. Bitterwolf, Coord. Chem. Rev. 206 (2000) 563.
[7] C. Tard, X.M. Liu, S.K. Ibrahim, M. Bruschi, L. De Gioia, S.C. Davies, X. Yang, L.S. Wang, G. Sawers, C.J. Pickett, Nature 433 (2005) 610.
[8] L.C. Song, Acc. Chem. Res. 38 (2005) 21.
[9] X.M. Liu, S.K. Ibrahim, C. Tard, C.J. Pickett, Coord. Chem. Rev. 249 (2005) 1641.
[10] J.F. Capon, F. Gloaguen, P. Schollhammer, J. Talarmin, Coord. Chem. Rev. 249 (2005) 1664.
[11] S.P. Best, Coord. Chem. Rev. 249 (2005) 1536.
[12] D.J. Evans, C.J. Pickett, Chem. Soc. Rev. 32 (2003) 268.
[13] L.C. Sun, B. Akermark, S. Ott, Coord. Chem. Rev. 249 (2005) 1653.
[14] F.F. Xu, C. Tard, X.F. Wang, S.K. Ibrahim, D.L. Hughes, W. Zhong, X.R. Zeng, Q.Y. Luo, X.M. Liu, C.J. Pickett, Chem. Commun. (2008) 606.
[15] X.F. Wang, Z.M. Li, X.R. Zeng, Q.Y. Luo, D.J. Evans, C.J. Pickett, X.M. Liu, Chem. Commun. (2008) 3555.
[16] C. Tard, X.M. Liu, D.L. Hughes, C.J. Pickett, Chem. Commun. (2005) 133.
[17] L.C. Song, H.T. Fan, Q.M. Hu, J. Am. Chem. Soc. 124 (2002) 4566.
[18] L.C. Song, J. Cheng, F.H. Gong, Q.M. Hu, J. Yan, Organometallics 24 (2005) 3764.
[19] L.C. Song, X.N. Fang, C.G. Li, J. Yan, H.L. Bao, Q.M. Hu, Organometallics 27 (2008) 3225.
[20] C. Kolomyjec, J. Whelan, B. Bosnich, Inorg. Chem. 22 (1983) 2343.
[21] A. Maisonnat, J. Devillers, R. Poilblanc, Inorg. Chem. 26 (1987) 1502.
[22] C.A. Ghilardi, S. Midollini, A. Orlandini, A. Vacca, J. Chem. Soc., Dalton Trans. (1993) 3117.
[23] C.A. Ghilardi, S. Midollini, A. Orlandini, G. Scapacci, Inorg. Chim. Acta 266 (1997) 113.
[24] M.H. Cheah, C. Tard, S.J. Borg, X.M. Liu, S.K. Ibrahim, C.J. Pickett, S.P. Best, J. Am. Chem. Soc. 129 (2007) 11085.
[25] L.C. Song, J. Cheng, J. Yan, H.T. Wang, X.F. Liu, Q.M. Hu, Organometallics 25 (2006) 1544.
[26] F. Gloaguen, J.D. Lawrence, M. Schmidt, S.R. Wilson, T.B. Rauchfuss, J. Am. Chem. Soc. 123 (2001) 12518.
[27] A. Winter, L. Zsolnai, G. Huttner, Z. Naturforsch. B 37 (1982) 1430.
[28] M. Razavet, S.C. Davies, D.L. Hughes, C.J. Pickett, Chem. Commun. (2001) 847.
[29] J.D. Lawrence, H.X. Li, T.B. Rauchfuss, Chem. Commun. (2001) 1482.
[30] M. Razavet, S.C. Davies, D.L. Hughes, J.E. Barclay, D.J. Evans, S.A. Fairhurst, X.M. Liu, C.J. Pickett, Dalton Trans. (2003) 586.

[31] C. Tard, Chemistry Related to the [Fe]-Hydrogenase, Department of Biological Chemistry, John Innes Centre, Norwich, 2005.
[32] G. Hogarth, M. O'Brien, D.A. Tocher, J. Organomet. Chem. 672 (2003) 29.
[33] X. Zhao, Y.M. Hsiao, C.H. Lai, J.H. Reibenspies, M.Y. Darensbourg, Inorg. Chem. 41 (2002) 699.
[34] X. Zhao, I.P. Georgakaki, M.L. Miller, R. Mejia-Rodriguez, C.Y. Chiang, M.Y. Darensbourg, Inorg. Chem. 41 (2002) 3917.
[35] S.J. George, Z. Cui, M. Razavet, C.J. Pickett, Chem. Eur. J. 8 (2002) 4037.
[36] E.J. Lyon, I.P. Georgakaki, J.H. Reibenspies, M.Y. Darensbourg, J. Am. Chem. Soc. 123 (2001) 3268.
[37] S. Ott, M. Kritikos, B. Akermark, L.C. Sun, R. Lomoth, Angew. Chem., Int. Ed. 43 (2004) 1006.
[38] I.P. Georgakaki, L.M. Thomson, E.J. Lyon, M.B. Hall, M.Y. Darensbourg, Coord. Chem. Rev. 238 (2003) 255.
[39] C.M. Thomas, M.Y. Darensbourg, M.B. Hall, J. Inorg. Biochem. 101 (2007) 1752.
[40] G. Zampella, M. Bruschi, P. Fantucci, M. Razavet, C.J. Pickett, L. De Gioia, Chem. Eur. J. 11 (2005) 509.
[41] Bruker, Bruker AX Inc., Madison, WI, USA, 2004.
[42] G.M. Sheldrick, SHELX-97-programs for crystal structure determination (SHELXS) and refinement (SHELXL), University of Göttingen, Germany, 1997.
[43] A.D. Becke, Phys. Rev. A 38 (1988) 3098.
[44] J.P. Perdew, Phys. Rev. B 33 (1986) 8822.
[45] A. Schafer, C. Huber, R. Ahlrichs, J. Chem. Phys. 100 (1994) 5829.
[46] R. Ahlrichs, M. Bar, M. Haeser, C. Horn, C. Kolmel, Chem. Phys. Lett. 162 (1989) 165.
[47] F. Jensen, Introduction to Computational Chemistry, John Wiley & Sons Ltd., Chichester, England, 1998.